

Fig. 10.1 A simple stereo camera geometry with parallel optical axes.

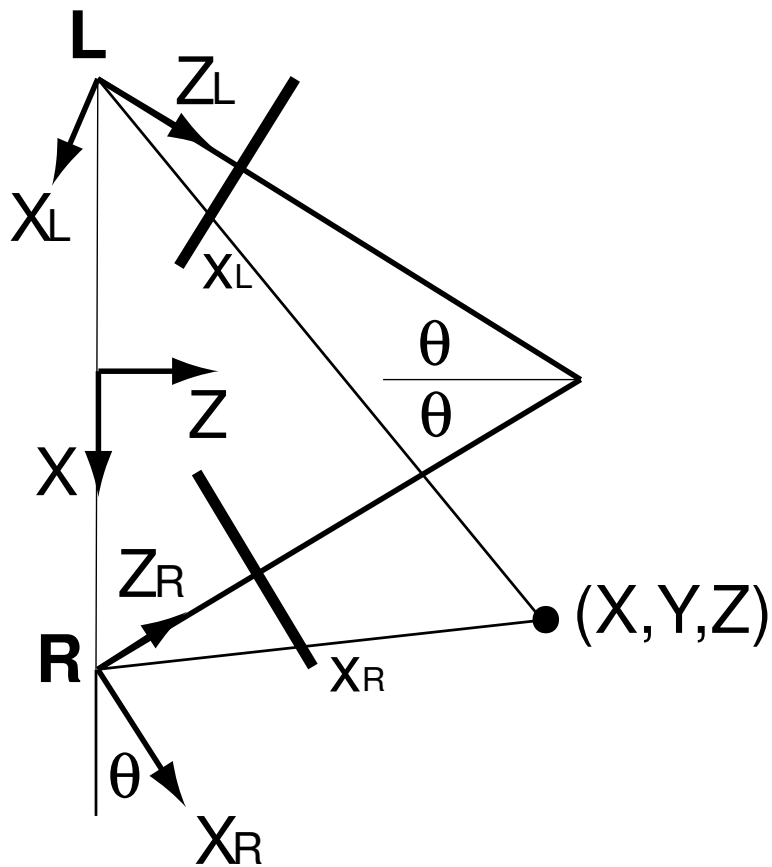


Fig. 10.2 A stereo camera geometry with converging optical axes.

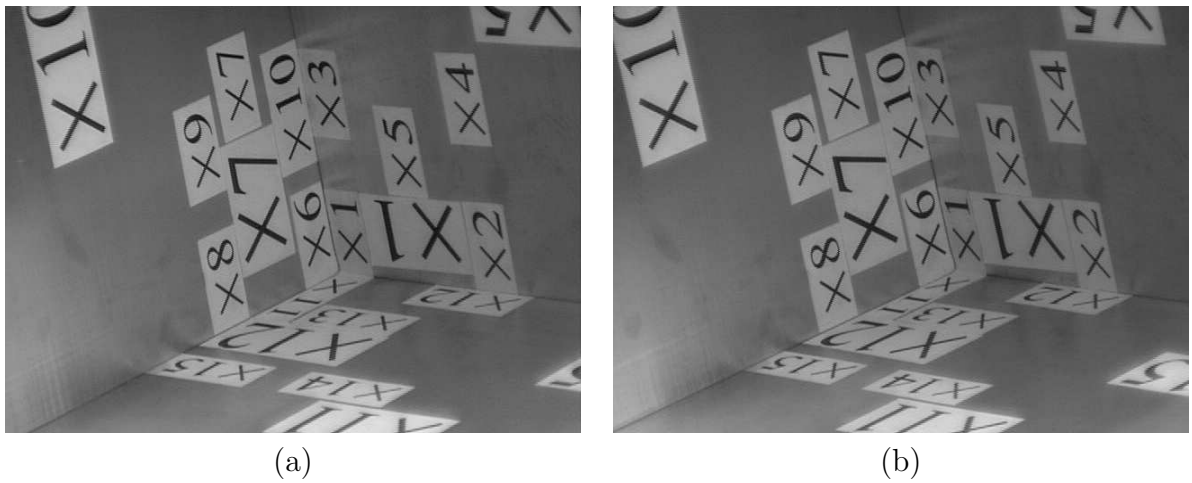


Fig. 10.3 (a), (b) Images of a calibration box obtained by a stereo camera system.

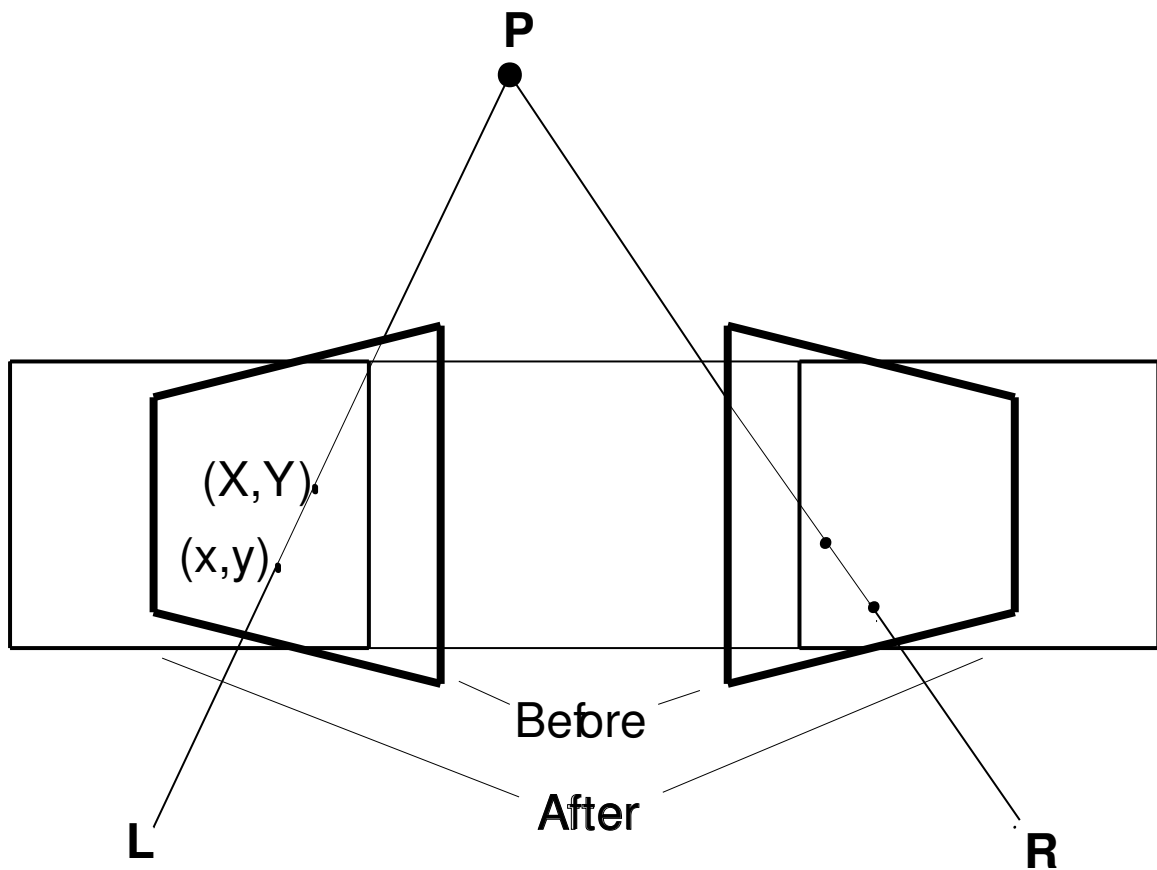


Fig. 10.4 Using two projective transformations, images obtained by converging optical axes are transformed to images as if obtained by cameras with parallel optical axes.

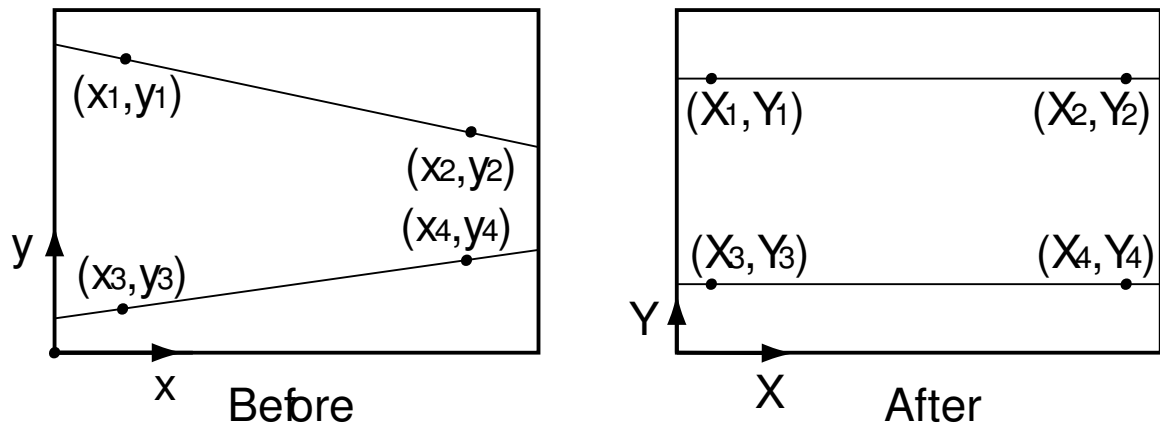
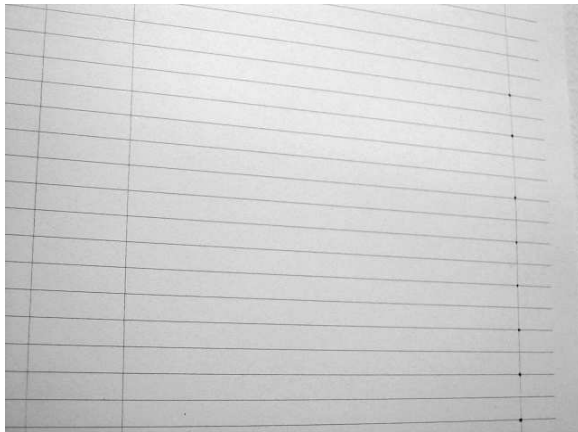
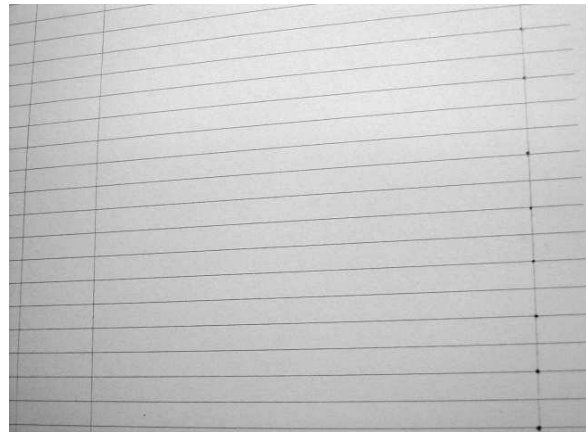


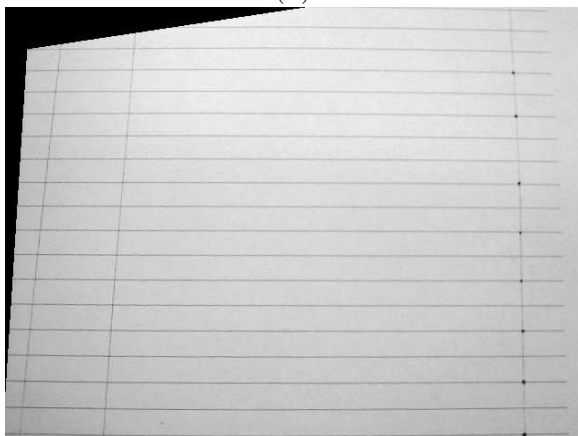
Fig. 10.5 Images before and after rectification.



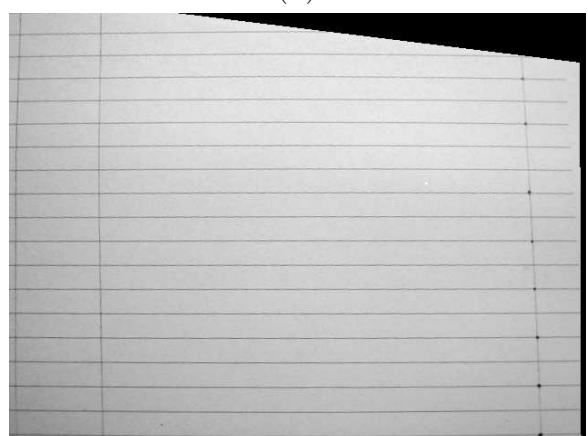
(a)



(b)



(c)



(d)

Fig. 10.6 (a), (b) Images of horizontal lines in 3-D parallel to the baseline obtained by a stereo camera system with converging optical axes. (c), (d) Rectification of the images so that corresponding epipolar lines fall on the same scanline in the images.

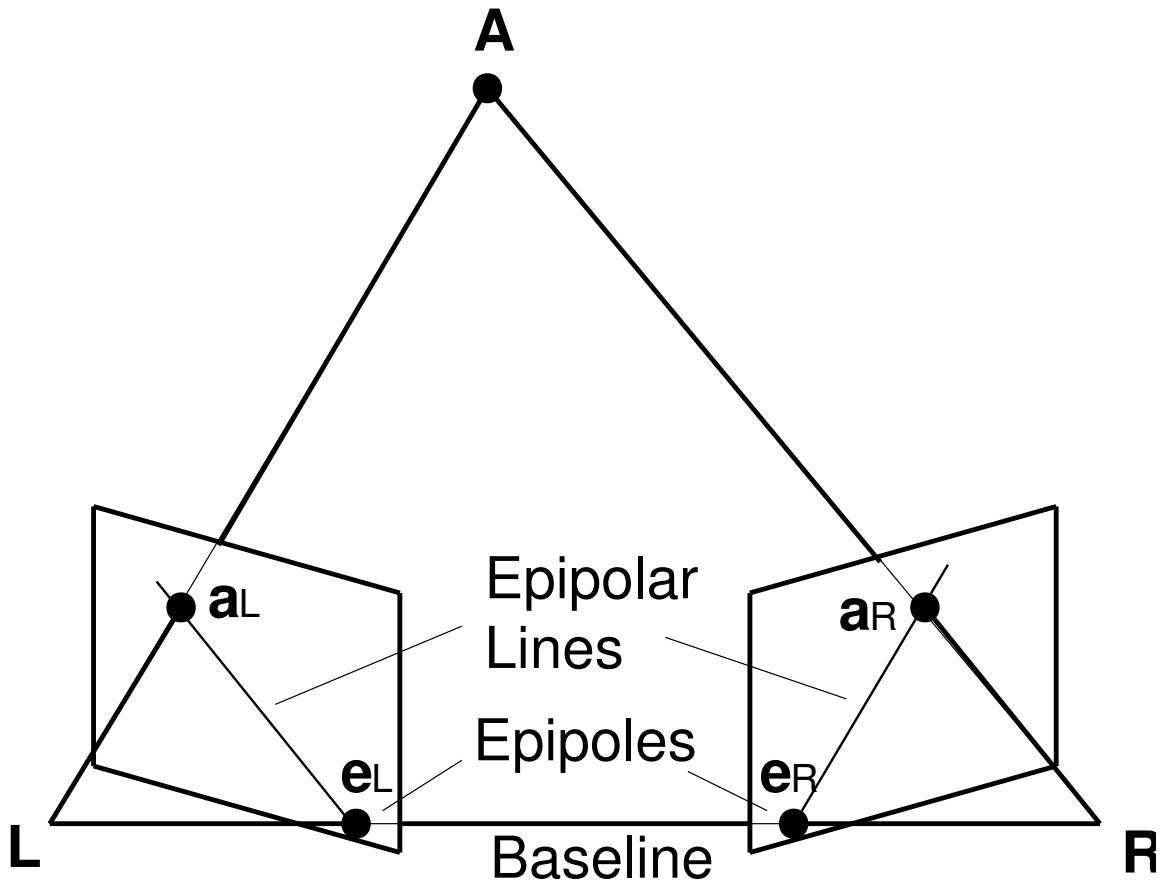


Fig. 10.7 The epipolar constraint in stereo images.

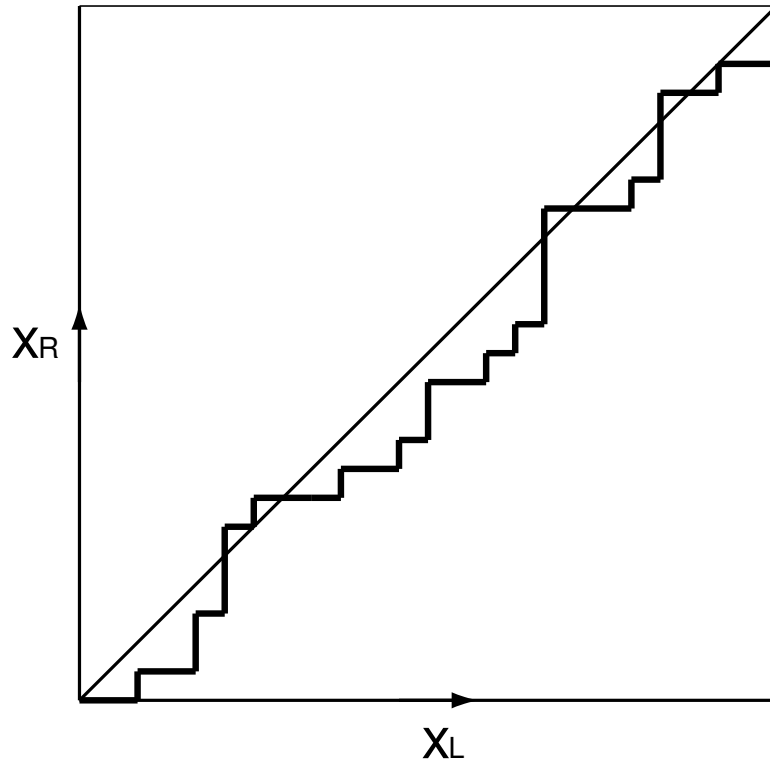


Fig. 10.8 Stereo correspondence by dynamic programming. The diagonal line shows the zero-disparity path, and the path shown by the contour represents a typical correspondence.

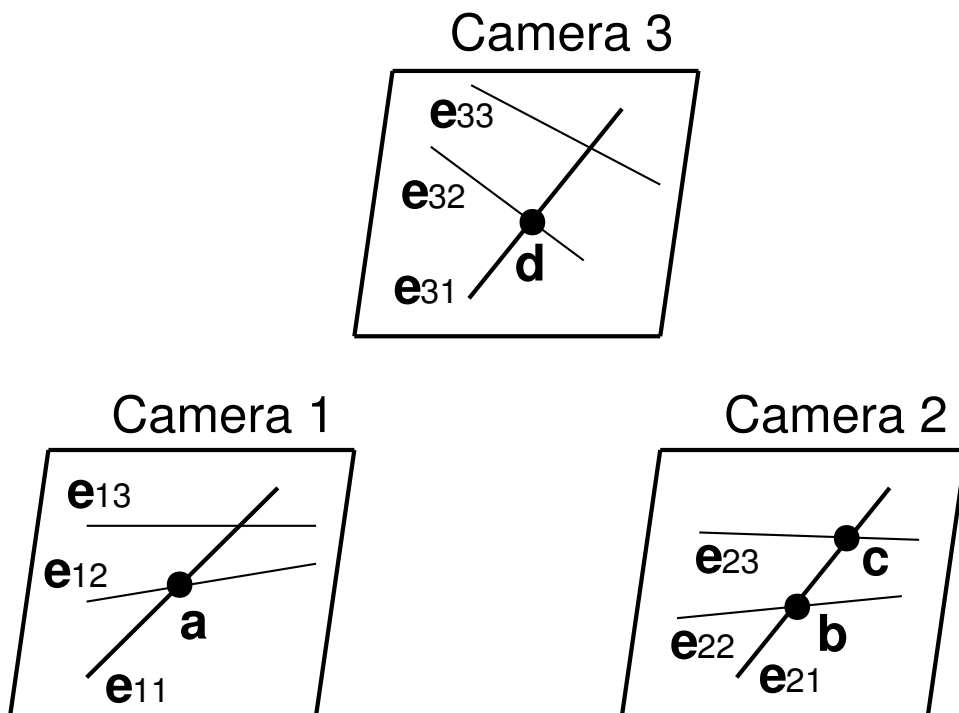


Fig. 10.9 The trinocular stereo geometry.

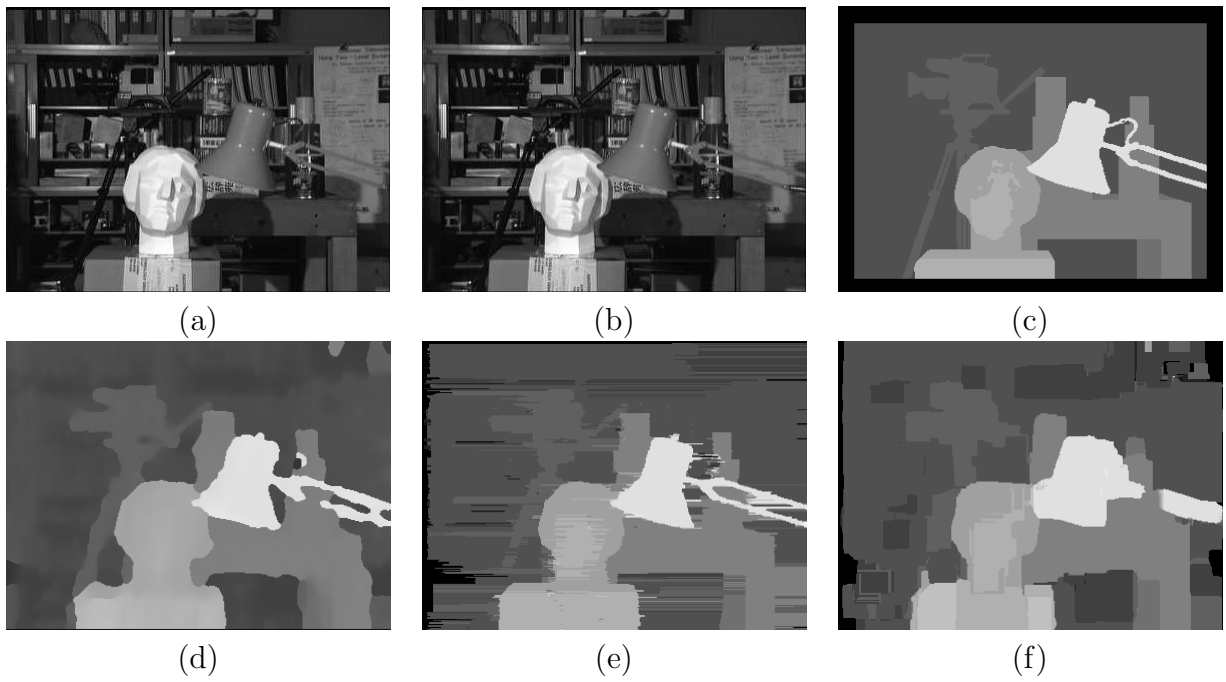


Fig. 10.10 (a), (b) The head-and-lamp stereo image pair. (c) The disparity ground truth. (d)–(f) Disparity maps obtained by an implementation of the cooperative algorithm, dynamic programming, and template matching, respectively.

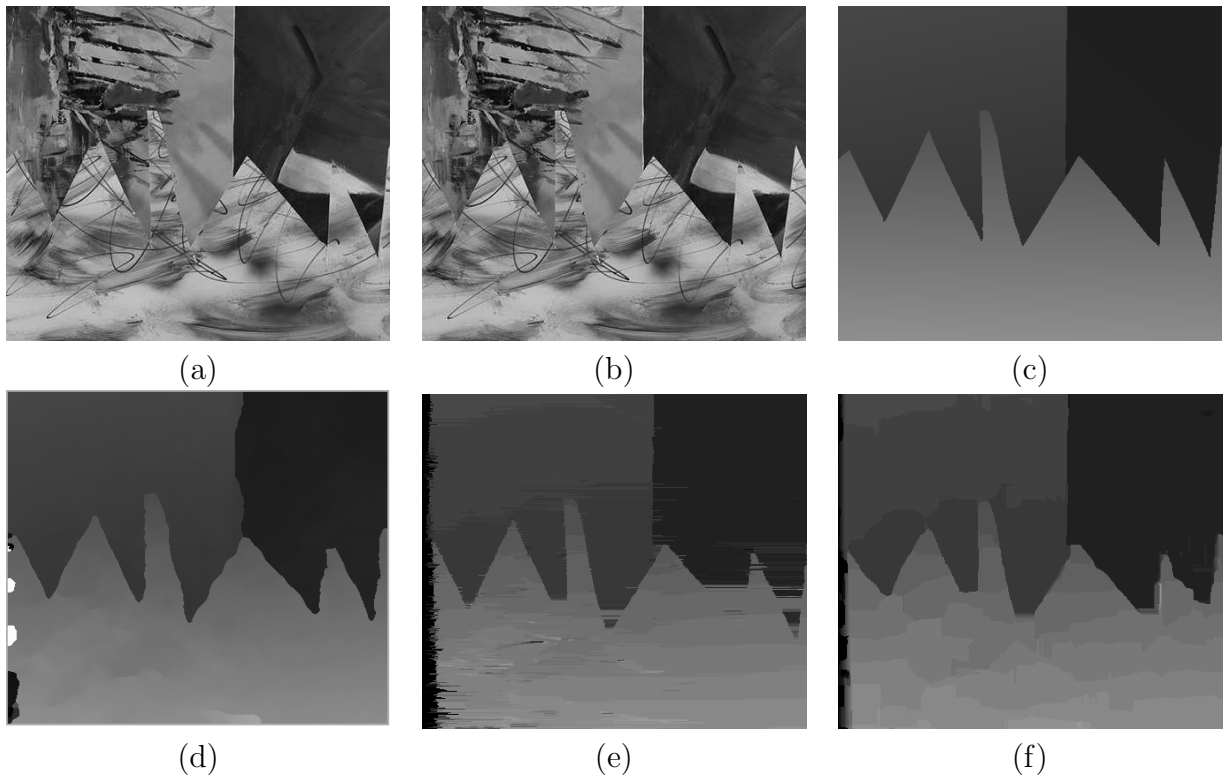


Fig. 10.11 (a), (b) The sawtooth stereo image pair. (c) Disparity ground truth. (d)–(f) Disparity maps obtained by the cooperative, dynamic programming, and template matching algorithms, respectively.

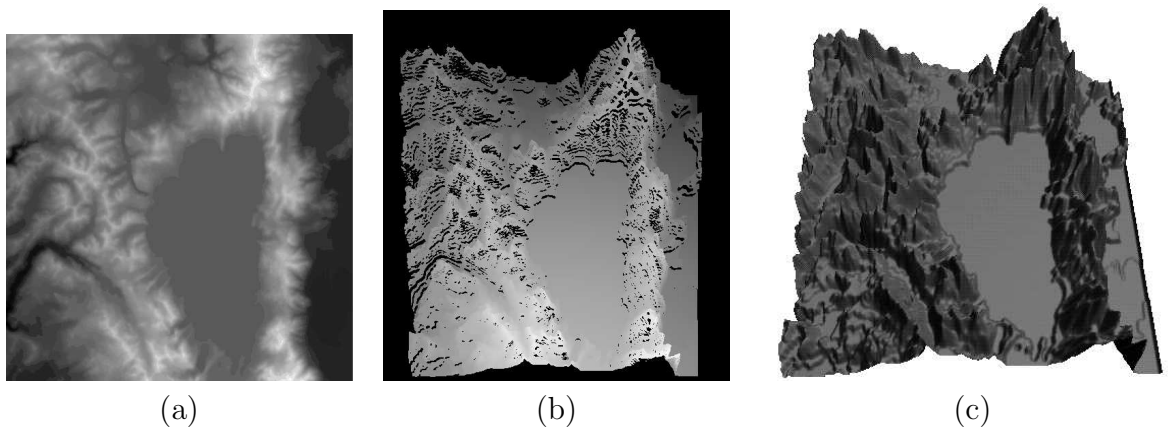


Fig. 10.12 (a) The top view of a depth map showing distances of scene points to the camera baseline; brighter pixels show scene points that are closer to the baseline. (b) The same depth map shown from the side. (c) Reconstruction of the scene by surface fitting.